

Article

Optomechanically Induced Transparency in Optomechanical System with a Cubic Anharmonic Oscillator

Weiyu Lv, Li Deng, Sumei Huang and Aixi Chen * 

School of Sciences and Department of Physics, Zhejiang Sci-Tech University, Hangzhou 310018, China

* Correspondence: aixichen@zstu.edu.cn

Abstract: In this paper, we studied the optomechanically induced transparency (OMIT) in a cavity optomechanical system containing a cubic nonlinear oscillator. In our system, a partially transparent, dielectric membrane was placed in the middle of the F-P cavity. Due to the partial transmission and reflective property of the membrane, the membrane was combined with both the mirrors on the left and right sides to form two cavities. When the system was driven by two coupling fields, we calculated the quantum fluctuation of the optomechanical system operators and showed the response of the cavity optomechanical system to the probe field. We found that the cubic nonlinearity led to a shift of the OMIT window, which moved towards a frequency less than the resonance frequency, and the absorption peak became significantly asymmetrical when OMIT appeared. The shift of the OMIT dip provided a method to detect the nonlinear effects of the system due to the existence of cubic anharmonic potential.

Keywords: cavity optomechanical; optomechanically induced transparency; cubic anharmonic oscillator

1. Introduction

In recent years, research into the cavity optomechanical system [1,2] has received more attention as a crossover research area between quantum optics and nano science. Studies about the cavity optomechanical system include the ground state cooling of mechanical oscillators [3,4], parametric normal-mode splitting [5,6], the preparation of non-classical states [7–9] and the slow light effect [10–12]. In the process of studying the cavity optomechanical system, Agarwal and his co-workers found the optomechanically induced transparency (OMIT) [13]. The optomechanically induced transparency was fairly similar to the electromagnetically induced transparency (EIT) [14]. We know that the electromagnetically induced transparency is a quantum coherent phenomenon: when a probe field interacts resonantly with a three-level atomic system driven by a strong coupling field, due to the quantum coherent control from the strong coupling field, coupling transition can occur, producing a pair of dressed state transitions. This changes the transition of the probe field into two transitions and leads destructive interference to absorption. Finally, the three-level atomic medium completely takes on the transparency phenomena for the probe field. EIT has become a quantum-manipulation technology widely used to manipulate quantum coherent media, based on the technology of EIT, double Fano resonance in a plasmonic double-grating structure [15], a plasmonic multilayer system [16] and metamaterial-induced transparency [17].

The theoretical scheme of OMIT was first proposed by Agarwal and Huang in 2010 in Ref. [13], and their studies showed how the probe field became transparent in optomechanical systems driven by a strong coupling field. Through the driving of this strong field, the first harmonic was generated. The reason for transparency was the occurrence of the destructive interference between the probe field and the first harmonic. In the year when the theory of OMIT was proposed, it was experimentally realized by Kippenberg's



Citation: Lv, W.; Deng, L.; Huang, S.; Chen, A. Optomechanically Induced Transparency in Optomechanical System with a Cubic Anharmonic Oscillator. *Photonics* **2023**, *10*, 407.

<https://doi.org/10.3390/photonics10040407>

Received: 8 February 2023

Revised: 1 April 2023

Accepted: 3 April 2023

Published: 5 April 2023



Copyright: © 2023 by the authors. Licensee MDPI, Basel, Switzerland. This article is an open access article distributed under the terms and conditions of the Creative Commons Attribution (CC BY) license (<https://creativecommons.org/licenses/by/4.0/>).

group [18]. Since then, OMIT has been considered for some physical systems, such as: superconducting loop systems [19]; Fabry–Perot optical cavities with semi-permeable film in the middle [20]; cascaded multimode-cavity optomechanical systems [21]; Bogoliubov mechanical modes [22]; cavity optomechanical systems with Kerr effect [23] and diamond optomechanical crystals [24]. Jing’s group obtained the optomechanically induced transparency in parity–time-symmetric microresonators [25]. Using the quantum manipulation of OMIT, the generation of second-order and higher-order sidebands in the cavity optomechanical system was reported [26–28]. In addition to the OMIT for a single probe field, researchers investigated two-color, electromagnetically induced transparency in a hybrid optomechanical system [29]. Alongside in-depth studies about OMIT, this quantum coherence phenomenon was extended to a micro-resonator, coupled with nanoparticles [30] and a spinning resonator [31]. Because of the extremely narrow transparency peak, OMIT has a wide range of applications in precision measurements [32,33].

The reason why the optomechanical system exhibits so many novel physical phenomena is due to the important role of quantum nonlinearity. By using the Duffing nonlinearity, Franco’s group investigated steady-state mechanical squeezing in an optomechanical system [34]. Regarding the coupling of the mechanical oscillator with the cavity field, the general processing mode is to treat the mechanical oscillator as a harmonic oscillator, meaning the mechanical oscillator has harmonic oscillator potential which is a quadratic function relating to position. In this work, we assumed that the mechanical oscillator had an anharmonic potential that included a cubic term besides the quadratic term of position. We investigated the optomechanically induced transparency of the optomechanical system, under the condition of the existence of a cubic anharmonic potential. We discussed the absorption and the dispersion spectrum of the output probe field in the system, under different strengths of mechanical nonlinearity and different values of other parameters. We found that the peak of the absorption and the dispersion spectrum will be asymmetric and the window of OMIT will deviate from the resonance point when a cubic nonlinearity oscillator exists in a system.

Our theoretical studies are based on current experimental progress in the field of cavity optomechanics. In order to numerically simulate the OMIT, our selections of parameters come from some experimental data. The research content of this paper is divided into three parts. In Section 2, we describe the physical model, give the Hamiltonian of the system, and obtain the steady-state expectation values of the system operators. Next, we explain how we calculated the quantum fluctuations of the operators and the steady conditions. Then, we explain how we obtained the response of the cavity optomechanical system to the probe field. In Section 3, we discuss influences of cubic anharmonic potential and other parameters on the absorption and the dispersion spectrum of the output probe field in the system. We briefly draw a conclusion in Section 4.

2. Physical Model and Methods

We considered a partially transparent membrane placed in the middle of a cavity. Due to the partial transmission and reflective property of the membrane, the membrane and the mirrors on the left and right sides of the cavity can form two cavities, respectively, as shown in Figure 1. The membrane coupled with the two optical cavities simultaneously. When the cavities were driven by strong coupling fields, mechanical motion of the membrane occurred due to the radiation pressure force. In this system, we assumed that the membrane had potential that included harmonic oscillator potential, as well as anharmonic potential which related to the function of cubic of position. Here, the membrane was called a cubic anharmonic oscillator [35], and it had nonlinear potential energy. In Figure 1, two strong coupling fields (two weak probe fields) with the same frequency ω_c (the frequency ω_p of the two weak probe fields) and amplitudes ε_c and ε_d (the amplitudes ε_p and ε_l of the two weak probe fields) were used to drive cavity a_1 and a_2 , respectively. This type of system has been studied on some phenomena in experiments [36–38].

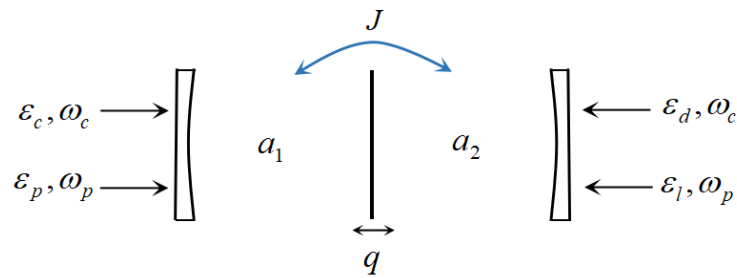


Figure 1. A three-mode optomechanical system, in which two cavities couple to a cubic anharmonic oscillator. Meanwhile, two cavities couple to each other with coupling strength J .

We describe the two optical cavities, respectively, by annihilation operators a_i and creation operators a_i^\dagger ($i = 1, 2$) while ω_i ($i = 1, 2$) are the resonance frequencies of the cavities and κ_i ($i = 1, 2$) are the decay rates of the cavities. The annihilation operators and creation operators are restricted by the commutation relation $[a_i, a_i^\dagger] = 1$. The mechanical oscillator, with a frequency ω_m and a damping rate γ_m , is described by displacement operator q and momentum operator p . These two operators satisfy the relation $[q, p] = i\hbar$. The Hamiltonian of the cubic anharmonic oscillator is then given by $H_m = m\omega_m^2 q^2/2 + p^2/2m + \alpha q^3/3$, where m denotes the effective mass of the oscillator, and α is the strength of the mechanical nonlinearity. Differences in α lead to different coupling-constant behavior [35]. It was found that the strength of the mechanical nonlinearity α can be about 11×10^7 N/m² in a system containing a movable mirror and a cubic anharmonic oscillator [39]. The first two terms in the above Hamiltonian represent the potential energy and kinetic energy of the harmonic oscillator, respectively, and the third term is the potential energy produced by the cubic mechanical nonlinearity. We write operators p and q as dimensionless momentum operator P and displacement operator Q . P and Q are defined by $p = \hbar/x_{zpf}$ and $q = x_{zpf}Q$, in which $x_{zpf} = \sqrt{\hbar/m\omega_m}$ is the amplitude of the zero-point motion of the mechanical oscillator and $h = 2\pi\hbar$ is Planck constant. P and Q satisfy the relation $[Q, P] = i$. Therefore, the Hamiltonian of the cubic anharmonic oscillator can be written as $H_m = \hbar\omega_m(Q^2 + P^2)/2 + \alpha\beta Q^3/3$, $\beta = x_{zpf}^3$. Since the cubic potential energy $\alpha\beta Q^3/3$ is much smaller than the quadratic potential energy, we can think of the cubic potential energy as a perturbation. In the rotating-wave frame of coupling frequency ω_c , the total Hamiltonian of the optomechanical system can be written as:

$$H = \hbar\Delta_1 a_1^\dagger a_1 + \hbar\Delta_2 a_2^\dagger a_2 + H_m + \hbar g_1 a_1^\dagger a_1 Q + \hbar g_2 a_2^\dagger a_2 Q + \hbar J(a_1^\dagger a_2 + a_2^\dagger a_1) + i\hbar\epsilon_c(a_1^\dagger - a_1) + i\hbar\epsilon_d(a_2^\dagger - a_2) + i\hbar\epsilon_p(a_1^\dagger e^{-i\delta t} - a_1 e^{i\delta t}) + i\hbar\epsilon_l(a_2^\dagger e^{-i\delta t} - a_2 e^{i\delta t}) \tag{1}$$

Here, $\Delta_i = \omega_i - \omega_c$ ($i = 1, 2$) are the detuning between cavities and coupling fields, and $\delta = \omega_p - \omega_c$ is the detuning between probe fields and coupling fields. The first and the second terms are the energy of two cavities. The fourth and fifth terms represent the interaction between the mechanical oscillator and the two optical cavities, respectively, which was caused by radiation pressure with the coupling strength $g_i = x_{zpf}\omega_i/l_i$ ($i = 1, 2$), with l_i being the length of cavities. The sixth term describes the Hamiltonian of the interaction between the two optical cavities. J is the coupling strength between the two cavities. The last four terms express the coupling of the coupling fields and the probe fields to the two optical cavities, respectively. The amplitudes of two coupling fields ϵ_d and ϵ_l are related to the decay rates κ_1 and κ_2 of the two optical cavity fields, the laser powers \wp_c and \wp_d and the frequency ω_c of input fields, so they are described as $\epsilon_c = \sqrt{2\kappa_1\wp_c/\hbar\omega_c}$ and $\epsilon_d = \sqrt{2\kappa_2\wp_d/\hbar\omega_d}$.

With the Hamiltonian written above in Equation (1), the dynamics of the system can be described by the quantum Langevin equation using the Heisenberg–Langevin equation:

$$\begin{aligned} \dot{a}_1 &= -i\Delta_1 a_1 - ig_1 a_1 Q - iJ a_2 + \varepsilon_c + \varepsilon_p e^{-i\delta t} - \kappa_1 a_1 + \sqrt{2\kappa_1} a_{1,in} \\ \dot{a}_2 &= -i\Delta_2 a_2 - ig_2 a_2 Q - iJ a_1 + \varepsilon_d + \varepsilon_l e^{-i\delta t} - \kappa_2 a_2 + \sqrt{2\kappa_2} a_{2,in} \\ Q &= \omega_m P \\ \dot{P} &= -g_1 a_1^\dagger a_1 - g_2 a_2^\dagger a_2 - \omega_m Q - \frac{\alpha\beta}{\hbar} Q^2 - \gamma_m P + \zeta \end{aligned} \tag{2}$$

Here, $a_{i,in}$ ($i = 1, 2$) is the input quantum vacuum noise in optical cavities with zero mean value $\langle a_{i,in} \rangle = 0$, and $\langle a_{i,in}(t) a_{i,in}^\dagger(t') \rangle = \delta(t - t')$ is the nonzero time-domain correlation function, while ζ is the thermal noise caused by the Brownian motion of the mechanical oscillator. The correlation function in the time domain is:

$$\langle \zeta(t) \zeta(t') \rangle = \frac{\gamma_m}{\omega_m} \int \frac{d\omega}{2\pi} \omega e^{-i\omega(t-t')} \left[1 + \coth\left(\frac{\hbar\omega}{2k_B T}\right) \right] \tag{3}$$

and its mean value is zero $\langle \zeta \rangle = 0$. In the above equation, k_B is the Boltzmann constant and T is the ambient temperature of the system. In this paper, we discuss the average response of the system to the input probe field; thus, the effect of the noise can be ignored in the subsequent calculations. Since the probe field, compared to the coupling field, is a weak field, the effect of the probe field can be regarded as a perturbation. Therefore, due to the perturbation effect of the probe field, each operator can be viewed as the sum of a steady-state mean value and small fluctuation, so we obtain $a_i = a_{is} + \delta a_i$, $Q = Q_s + \delta Q$, $P = P_s + \delta P$. The steady-state mean value is related to the input coupling field. In the absence of probe fields ε_p and ε_l , we can obtain the steady-state mean values of operators in the system:

$$\begin{aligned} a_{1s} &= \frac{\varepsilon_c(i\Delta'_2 + \kappa_2) - iJ\varepsilon_d}{(i\Delta'_1 + \kappa_1)(i\Delta'_2 + \kappa_2) + J^2} \\ a_{2s} &= \frac{\varepsilon_d(i\Delta'_1 + \kappa_1) - iJ\varepsilon_c}{(i\Delta'_1 + \kappa_1)(i\Delta'_2 + \kappa_2) + J^2} \\ Q_s &= \frac{-ig_1|a_{1s}|^2 - ig_2|a_{2s}|^2}{\omega_m + \frac{\alpha\beta}{\hbar} Q_s} \\ P_s &= 0 \end{aligned} \tag{4}$$

With $\Delta'_i = \Delta_i + g_i Q_s$ ($i = 1, 2$) denoting the effective detuning between two cavities and coupling fields, respectively, $g_i Q_s$ is the optomechanical coupling strength of the mechanical oscillator and the two cavities, respectively. It can be noticed from the above equations that the steady-state mean value of the mechanical oscillator Q_s depends on the mechanical nonlinearity strength α and the number of cavity photons $|a_{is}|^2$.

The quantum Langevin equations in Equation (2) are nonlinear equations, so we solve them by keeping the only linear terms of fluctuation operators and ignoring quadratic higher-order fluctuation. Therefore, the linearized quantum Langevin equations of fluctuation operators are shown as:

$$\begin{aligned} \dot{\delta a}_1 &= -i\Delta'_1 \delta a_1 - ig_1 a_{1s} \delta Q - iJ \delta a_2 - \kappa_1 \delta a_1 + \varepsilon_p e^{-i\delta t} \\ \dot{\delta a}_2 &= -i\Delta'_2 \delta a_2 - ig_2 a_{2s} \delta Q - iJ \delta a_1 - \kappa_2 \delta a_2 + \varepsilon_l e^{-i\delta t} \\ \delta Q &= \omega_m \delta P \\ \dot{\delta P} &= -g_1 a_{1s} \delta a_1^\dagger - g_1 a_{1s}^* \delta a_1 - g_2 a_{2s} \delta a_2^\dagger - g_2 a_{2s}^* \delta a_2 - \omega_m \delta Q - 2\frac{\alpha\beta}{\hbar} Q_s \delta Q - \gamma_m \delta P \end{aligned} \tag{5}$$

Due to the presence of the operators δa_i^\dagger , the amplitude and phase quadrature fluctuation operators of the cavities are introduced as $\delta x_1 = (\delta a_1 + \delta a_1^\dagger) / \sqrt{2}$, $\delta x_2 = (\delta a_2 + \delta a_2^\dagger) / \sqrt{2}$,

$\delta y_1 = (\delta a_1 - \delta a_1^\dagger) / (i\sqrt{2})$, $\delta y_2 = (\delta a_2 - \delta a_2^\dagger) / (i\sqrt{2})$. The Langevin equations above in Equation (5) therefore can be written in the following matrix form:

$$\dot{f}(t) = \mathbf{M}f(t) + f_{in} \tag{6}$$

where $f(t)$, f_{in} and the coefficient matrix \mathbf{M} in Equation (6) are shown as follows:

$$\begin{aligned} f(t) &= (\delta x_1, \delta x_2, \delta y_1, \delta y_2, \delta Q, \delta P)^T \\ f_{in} &= (x_{1,in}, x_{2,in}, y_{1,in}, y_{2,in}, 0, 0)^T \\ \mathbf{M} &= \begin{pmatrix} -\kappa_1 & 0 & \Delta'_1 & J & g_1 v_1 & 0 \\ 0 & -\kappa_2 & J & \Delta'_2 & g_2 v_2 & 0 \\ -\Delta'_1 & -J & -\kappa_1 & 0 & -g_1 u_1 & 0 \\ -J & -\Delta'_2 & 0 & -\kappa_2 & -g_2 u_2 & 0 \\ 0 & 0 & 0 & 0 & 0 & \omega_m \\ -g_1 u_1 & -g_2 u_2 & -g_1 v_1 & -g_2 v_2 & -\omega_m - 2\frac{\alpha\beta}{\hbar} Q_s & -\gamma_m \end{pmatrix} \end{aligned} \tag{7}$$

Here, $u_1 = (a_{1s} + a_{1s}^*) / \sqrt{2}$, $u_2 = (a_{2s} + a_{2s}^*) / \sqrt{2}$, $v_1 = (a_{1s} - a_{1s}^*) / (i\sqrt{2})$, $v_2 = (a_{2s} - a_{2s}^*) / (i\sqrt{2})$, $x_{1,in} = (\varepsilon_p e^{-i\delta t} + \varepsilon_p e^{i\delta t}) / \sqrt{2}$, $x_{2,in} = (\varepsilon_l e^{-i\delta t} + \varepsilon_l e^{i\delta t}) / \sqrt{2}$, $y_{1,in} = (\varepsilon_p e^{-i\delta t} - \varepsilon_p e^{i\delta t}) / (i\sqrt{2})$, $y_{2,in} = (\varepsilon_l e^{-i\delta t} - \varepsilon_l e^{i\delta t}) / (i\sqrt{2})$. When the real parts of the eigenvalues of the coefficient matrix \mathbf{M} are negative, the system may be in a steady state. We can use the method of the Routh–Hurwitz stability criterion [40] to derive the stability conditions for the system. In the following discussion, it is necessary to make reasonable choices and adjustments to ensure that the system is always in a steady state.

For simplicity of calculation, we assumed that the membrane was a perfect semi-transmissive and semi-reflective membrane, and we let the amplitudes of the two probe fields be equal, that is, we let $\varepsilon_l = \varepsilon_p$. This was under the assumption that it was reasonable to expand the fluctuation operators by the perturbation method, as the form $\delta w = w_+ \varepsilon_p e^{-i\delta t} + w_- \varepsilon_p e^{i\delta t}$, where $w = a_1, a_2, Q, P$. If we substitute the form of every operator into Equation (5), it can be solved as follows:

$$\begin{aligned} a_{1+} &= \frac{-ig_1 a_{1s} Q_+ - iJ a_{2+} + 1}{\kappa_1 + i\Delta'_1 - i\delta} \\ a_{2+} &= \frac{-ig_2 a_{2s} Q_+ - iJ a_{1+} + 1}{\kappa_2 + i\Delta'_2 - i\delta} \\ Q_+ &= \frac{\omega_m}{-i\delta} P_+ \\ P_+ &= \frac{i}{\delta} \left(-g_1 a_{1s} a_{1-}^* - g_1 a_{1s}^* a_{1+} - g_2 a_{2s} a_{2-}^* - g_2 a_{2s}^* a_{2+} - \omega_m Q_+ - 2\frac{\alpha\beta}{\hbar} Q_s Q_+ - \gamma_m P_+ \right) \end{aligned} \tag{8}$$

With further calculations, output fields for both cavities can be obtained from:

$$\begin{aligned} a_{1+} &= \frac{(L_2 + N_2)B}{N_1 N_2 - L_1 L_2} \\ a_{2+} &= \frac{(L_1 + N_1)B}{N_1 N_2 - L_1 L_2} \end{aligned} \tag{9}$$

where

$$\begin{aligned} A &= -\frac{\delta^2}{\omega_m} - \frac{i\delta\gamma_m}{\omega_m} + \omega_m + \frac{2\alpha\beta}{\hbar} Q_s \\ B &= A(\kappa_1 - i\Delta'_1 - i\delta)(\kappa_2 - i\Delta'_2 - i\delta) + ig_1^2 |a_{1s}|^2 (\kappa_2 - i\Delta'_2 - i\delta) + ig_2^2 |a_{2s}|^2 (\kappa_1 - i\Delta'_1 - i\delta) \\ S_1 &= [g_1 a_{1s}^* (\kappa_2 - i\Delta'_2 - i\delta) + iJ g_2 a_{2s}] (\kappa_1 - i\Delta'_1 - i\delta) \\ S_2 &= [g_2 a_{2s}^* (\kappa_1 - i\Delta'_1 - i\delta) + iJ g_1 a_{1s}] (\kappa_2 - i\Delta'_2 - i\delta) \\ L_1 &= ig_2 a_{2s} S_1 - iJB \\ L_2 &= ig_1 a_{1s} S_2 - iJB \\ N_1 &= B(\kappa_1 + i\Delta'_1 - i\delta) - ig_1 a_{1s} S_1 \\ N_2 &= B(\kappa_2 + i\Delta'_2 - i\delta) - ig_2 a_{2s} S_2 \end{aligned} \tag{10}$$

For studying the output fields of both two cavities, we needed to work out the output fields a_{out1} and a_{out2} , which can be obtained according to the input–output relation [18] $a_{in} + a_{out} = 2\kappa\delta a$. From the model, we found that the input fields were $a_{in,1} = \varepsilon_c + \varepsilon_p e^{-i\delta t}$ and $a_{in,2} = \varepsilon_d + \varepsilon_l e^{-i\delta t}$. Therefore, the output fields of this system were written as Equation (11):

$$\begin{aligned} a_{out1} + \varepsilon_c + \varepsilon_p e^{-i\delta t} &= 2\kappa_1\delta a_1 \\ a_{out2} + \varepsilon_d + \varepsilon_l e^{-i\delta t} &= 2\kappa_2\delta a_2 \end{aligned} \tag{11}$$

Meanwhile, we expanded the output fields into the form of $a_{out} = a_+ \varepsilon_p e^{-i\delta t} + a_- \varepsilon_p e^{i\delta t}$ in the same way. Combined with the input–output relationship, the output response corresponding to the probe fields of the two cavities can be obtained as:

$$\begin{aligned} \varepsilon_{out1+} &= 2\kappa_1 a_{1+} - 1 \\ \varepsilon_{out2+} &= 2\kappa_2 a_{2+} - 1 \end{aligned} \tag{12}$$

We characterized the properties of the output probe fields by quadrature of the fields $\varepsilon_{T1} = 2\kappa_1 a_{1+}$ and $\varepsilon_{T2} = 2\kappa_2 a_{2+}$, where the real part represents the absorption property, and the imaginary part represents the dispersion property [17].

3. Discussion and Results

For this study, we first focused on the relationship between the ratio of the cubic potential energy to the quadratic potential energy of the mechanical oscillator and the mechanical nonlinearity strength α . We assumed each coupling field drove cavities at the red-detuned mechanical sideband, making the effective detuning $\Delta'_1 = \Delta'_2 = \Delta' \approx \omega_m$ and set $x = \delta - \omega_m$. Due to the steady condition, we referred to a study which has been worked out [6], and the specific parameters were selected as follows: the frequencies of the input coupling fields are $\omega_c = \omega_d = 2\pi \times 6.07$ GHz; the frequency of the mechanical oscillator is $\omega_m = 2\pi \times 1.45$ MHz; the effective mass of the mechanical oscillator is $m = 12$ pg; the coupling strength between the cavities and the mechanical oscillator is $g_1 = g_2 = g = 2\pi \times 1.26\sqrt{3}$ Hz; the decay rate of the cavities is $\kappa_1 = \kappa_2 = \kappa = 0.1\omega_m$; the damping rate of the mechanical oscillator is $\gamma_m = 2\pi \times 24$ Hz; the coupling strength between two cavities is $J = 2\pi \times 12.5$ kHz and the power of the input coupling fields is $\wp_c = \wp_d = 2$ μ w. It can be seen from Equations (9) and (10) that the output probe fields of the two cavities are the same under this set of parameters, which can be written as $\varepsilon_{T1} = \varepsilon_{T2} = \varepsilon_T$. Figure 2 shows the ratio of the cubic potential energy to the quadratic potential energy of the mechanical oscillator as a function of the mechanical nonlinearity strength α . When the nonlinear strength α increases from 0 to 12×10^7 N/m², the ratio of the cubic potential energy to the quadratic potential energy $r = |\alpha\beta Q_s^3/3|/(m\hbar Q_s^2/2)$ increases as α increases. When the mechanical nonlinearity strength reaches $\alpha = 12 \times 10^7$ N/m², the ratio becomes $|\alpha\beta Q_s^3/3|/(m\hbar Q_s^2/2) \approx 0.093$, which means the cubic potential energy is much smaller than the quadratic potential energy at steady state and can be regarded as a perturbation.

Next, we discuss the optomechanically induced transparency of the system containing a cubic anharmonic oscillator. We first considered the influence of the mechanical nonlinearity strength α on the output probe field spectrum of the cubic potential energy contained in the mechanical oscillator. We plotted the real and the imaginary parts of the output field amplitude ε_T versus the normalized frequency x/ω_m for different mechanical nonlinearity strength $\alpha = 0$, $\alpha = 5 \times 10^7$ N/m² and $\alpha = 12 \times 10^7$ N/m². Here, Figure 3a shows the real part of the output field amplitude ε_T , and Figure 3b shows the imaginary part of the output field amplitude ε_T . As shown in Figure 3a, there is a dip near $x = 0$ where the detuning is $\delta = \omega_m$ as $\alpha = 0$. That is to say, the absorption effect of the optical system on the probe field is zero at the resonance when the mechanical nonlinearity strength is absent. The value of ε_T is close to zero, and this means that the input probe field transmitted completely through the system without loss. With the increase in the mechanical nonlinearity strength, the two absorption peaks gradually become asymmetric; one absorption peak becomes higher and

narrower, and the other absorption peak becomes lower and broader. At the same time, the positions of the two absorption peaks are shifted to the left, and the window width of the OMIT is slightly broader and is also shifted to the left and gradually deviated from the resonance point. The dispersion spectrum of the output field amplitude ε_T is shown as Figure 3b, and its slope represents the group delay. From the figure, we can see that as the mechanical nonlinearity strength increased, and the slope of the dispersion curve gradually decreased, which means the group delay became smaller near the point where the OMIT occurred.

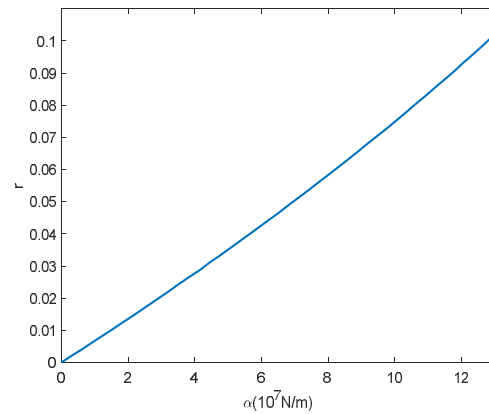


Figure 2. The ratio of the cubic potential energy to the quadratic potential energy of the mechanical oscillator $r = |\alpha\beta Q_s^3/3| / (m\hbar Q_s^2/2)$ as a function of the mechanical nonlinearity strength α .

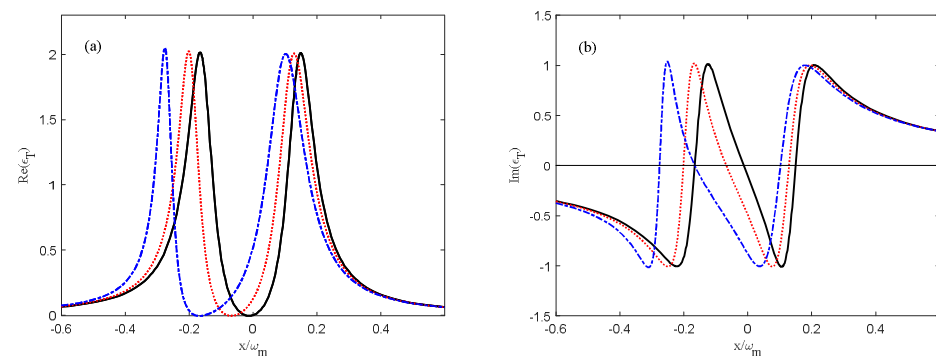


Figure 3. The output probe field amplitude ε_T as a function of normalized detuning x/ω_m for different mechanical nonlinearity strength α . (a) Absorption spectrum. (b) Dispersion spectrum. Black solid line, red dotted line and blue dashed line represent the mechanical nonlinearity strength $\alpha = 0$, $\alpha = 5 \times 10^7 \text{ N/m}^2$, and $\alpha = 12 \times 10^7 \text{ N/m}^2$, respectively.

Next, we discuss the differences between the spectrum of our OMIT and that of the standard OMIT in Ref. [13]. In previous work [13], the potential energy of a mechanical oscillator was $\hbar\omega_m Q^2/2$. In this case, when the oscillator was driven by the coupling field with frequency ω_c , it oscillated with the frequency ω_m , and the system generated harmonic wave with frequency $\omega_m + \omega_c$. If the $\omega_m + \omega_c$ was equal to frequency ω_p of the probe field, interference phenomenon occurred and the system could display a transparent window with two symmetrically distributed absorption peaks on both sides of the window, which is called the OMIT. However, in our paper, we considered that the membrane was in the potential energy with $\hbar\omega_m Q^2/2 + \alpha\beta Q^3/3$ which no longer represented a harmonic oscillator potential. The cubic anharmonic potential $\alpha\beta Q^3/3$ changed the membrane's oscillation frequency that was no longer equal to ω_m , so the position of the transparent window would shift, while the two absorption peaks were no longer strictly symmetrically changing the values of α .

We plotted the output probe field amplitude ε_T as a function of normalized detuning x/ω_m for different decay rates κ of the optical cavity field in Figure 4. We chose the mechanical nonlinearity strength $\alpha = 5 \times 10^7$ N/m² for the discussion of this part, and other parameters were the same as in Figure 3. We focused on the corresponding output probe fields when the decay rates κ were $\kappa = 0.02\omega_m$, $\kappa = 0.05\omega_m$ and $\kappa = 0.1\omega_m$. It can be observed that the two absorption peaks became narrower gradually and had a slight tendency to become lower as the decay rate κ became smaller and contracted towards the resonance point. The window width of OMIT became narrower, and the point where the OMIT appears shifted gradually to the right and closed towards the resonance point. In Figure 4b, we find that the corresponding dispersion curve near the point where the absorption was zero became steeper as the decay rate decreased, and its slope increased as the decay rate decreased.

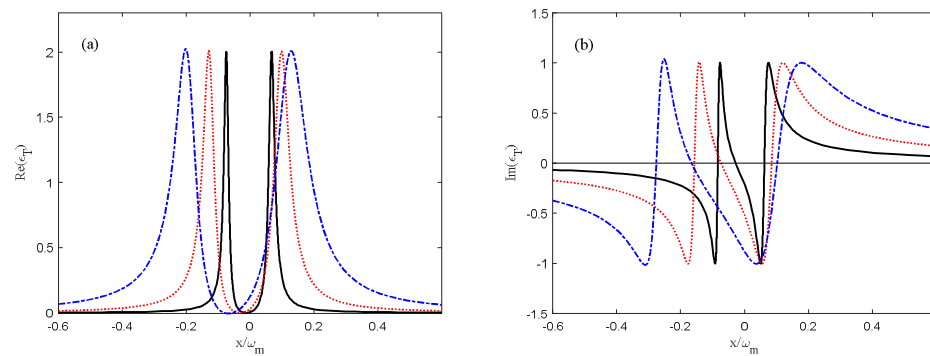


Figure 4. The output probe field amplitude ε_T as a function of normalized detuning x/ω_m for different decay rates κ of the optical cavity field. (a) Absorption spectrum. (b) Dispersion spectrum. Black solid line, red dotted line and blue dashed line represent the decay rate $\kappa = 0.02\omega_m$, $\kappa = 0.05\omega_m$ and $\kappa = 0.1\omega_m$, respectively.

In addition to this, it can be seen that the coupling strength g between the cavities and the oscillator, and the coupling strength J between the two cavities are also factors affecting the output probe fields. In Figure 5, we show the output probe field amplitude ε_T as a function of normalized detuning x/ω_m when the coupling strength g between the cavities and the oscillator were $g = 2\pi \times 1.26 \times 0.5$ Hz, $g = 2\pi \times 1.26$ Hz and $g = 2\pi \times 1.26\sqrt{3}$ Hz. Mechanical nonlinearity strength $\alpha = 5 \times 10^7$ N/m² was considered here, while the other parameters were the same as in Figure 3. When the coupling strength g became smaller, the two absorption peaks became lower and moved close to the resonance point, forming a narrower OMIT dip which also moved to the resonance point. The trend of the output probe field spectrum was similar to Figure 4, but the reduction in g could make the OMIT dip of the output field become narrower than in Figure 4. The dispersion spectrum of the output probe field is plotted in Figure 5b. We found that near the detuning corresponding to the OMIT dip, the slope of the curve became steeper as g became smaller.

Finally, we discuss the influence of the coupling strength J between the two cavities on output probe field ε_T which is a function of normalized detuning x/ω_m in Figure 6. We chose the coupling strengths $J = 2\pi \times 12.5$ kHz, $J = 2\pi \times 92.5$ kHz and $J = 2\pi \times 225$ kHz. When the coupling strength J decreased, the two absorption peaks obviously became asymmetric. The absorption peak on the left became higher and wider and gradually moved away from the resonance point, while the absorption peak on the right became lower and narrower and moved towards the resonance point. Differing from the above discussion, the decrease in J made the OMIT dip move towards to the left and away from the resonance point. In addition to this, the slope of the corresponding dispersion curve gradually became gentler as the coupling strength J between the two cavities decreased.

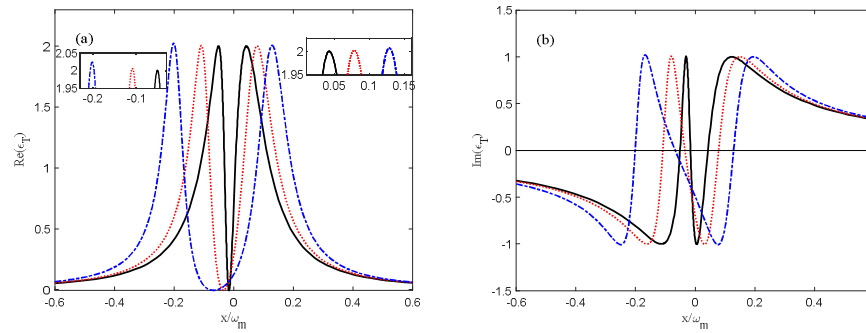


Figure 5. The output probe field amplitude ϵ_T as a function of normalized detuning x/ω_m for different coupling strength g between the cavities and the oscillator. (a) Absorption spectrum. (b) Dispersion spectrum. Black solid line, red dotted line and blue dashed line represent the coupling strength $g = 2\pi \times 1.26 \times 0.5$ Hz, $g = 2\pi \times 1.26$ Hz and $g = 2\pi \times 1.26\sqrt{3}$ Hz, respectively.

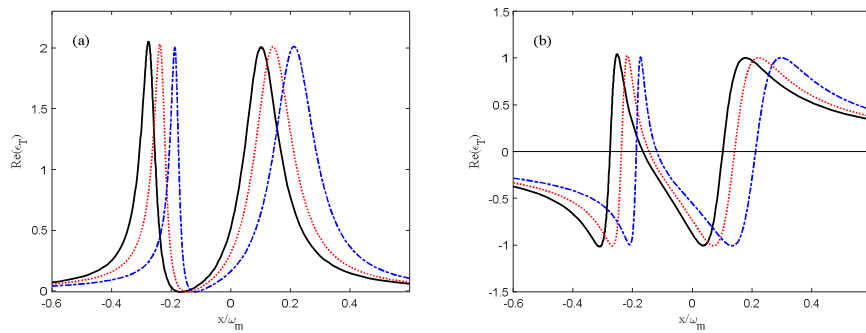


Figure 6. The output probe field amplitude ϵ_T as a function of normalized detuning x/ω_m for different coupling strength J between the two cavities. (a) Absorption spectrum. (b) Dispersion spectrum. Black solid line, red dotted line and blue dashed line represent the coupling strength $J = 2\pi \times 12.5$ kHz, $J = 2\pi \times 92.5$ kHz and $J = 2\pi \times 225$ kHz, respectively.

4. Conclusions

Many phenomena have been achieved in the system with two cavities and an oscillator, such as coherent perfect absorption (CPA), coherent perfect transmission (CPT) and coherent perfect synthesis (CPS) [41]. In this paper, we investigated the OMIT of the cavity optomechanical system containing a cubic anharmonic oscillator. We found that the presence of the cubic nonlinear anharmonic oscillator made the absorption spectrum of the output probe field become asymmetric and caused the OMIT dip to move away from the resonance point. These phenomena became stronger with the increase in the mechanical nonlinearity strength α . Moreover, in the cavity optomechanical system with a cubic anharmonic oscillator, the decay rate of the cavity field, the coupling strength between the two optical cavities and the coupling strength between the cavities and the mechanical oscillator all affected the absorption peak of the output probe field and the position of the OMIT dip. Among these, a smaller decay rate of the cavity field, or a smaller coupling strength between the two optical cavities and the mechanical oscillator led to a narrower OMIT dip, and the effective detuning where the OMIT occurred was closer to the resonance point $\delta = \omega_m$. On the contrary, the effective detuning moved away from the resonance point $\delta = \omega_m$ where the OMIT occurred if the coupling strength between the two optical cavities decreased, even though the window width of OMIT was also slightly narrower. Besides this, the coupling strength between the two optical cavities also lead to a more obviously asymmetric phenomenon of the absorption peak, but it was opposite to the trend of the absorption peak height when the mechanical nonlinearity strength increased. Therefore, we found that we could adjust the position and width of the transparent window to achieve the OMIT required for different applications in this system. These results show that the

influences of the cubic anharmonic potential on the spectrum of OMIT are significant, so we can detect the nonlinearity strength of the mechanical oscillator by measuring the shift of the transparent window. Our studies show the existence of cubic anharmonic potential to enhance the nonlinearity of the cavity optomechanical system; therefore, we can also extend this effect to the study of slow light and optical second-order sideband. Future research can also be extended to studying optomechanically induced amplification and optomechanically induced absorption, which provides optical information processing techniques for all-optical communication networks. Finally, we discuss the experimental feasibility of our scheme. With the development of micro/nano electromechanical technology, the optomechanical system has developed rapidly in recent years, and the parameters and scales of optomechanical systems have crossed the boundary between macro and micro. The oscillation frequency and effective mass values of the mechanical oscillator cover a very wide range, ranging from 10 to 10^9 Hz and from 10^3 to 10^{-20} g, respectively. Electromagnetic radiation also spans the wavebands of microwaves and optical waves. In this paper, the frequencies of the input coupling fields were $\omega_c = \omega_d = 2\pi \times 6.07$ GHz, the frequency of the mechanical oscillator was $\omega_m = 2\pi \times 1.45$ MHz, and the effective mass of the mechanical oscillator was $m = 12$ pg. Based on the current development of cavity optomechanical technology, maybe our scheme could be feasible for use in experiments.

Author Contributions: Conceptualization and model, S.H. and A.C.; numerical simulation, W.L. and L.D.; writing—original draft preparation, W.L. and S.H.; writing—review and editing, L.D. and A.C. All authors have read and agreed to the published version of the manuscript.

Funding: This research was supported by the National Natural Science Foundation of China through Grants No. 12175199, and No. 12174344, Zhejiang Provincial Natural Science Foundation of China through Grant No. LZ20A040002, and No. LY21A040007, and the Science Foundation of Zhejiang Sci-Tech University through Grants No. 19062408-Y and No. 17062071-Y.

Institutional Review Board Statement: Not applicable.

Informed Consent Statement: Not applicable.

Data Availability Statement: Not applicable.

Conflicts of Interest: The authors declare no conflict of interest.

References

1. Haroche, S.; Kleppner, D. Quantum cavity electrodynamics. *Phys. Today* **1989**, *42*, 24. [[CrossRef](#)]
2. Mabuchi, H.; Doherty, A.C. Quantum cavity electrodynamics: Coherence in context. *Science* **2002**, *298*, 1372–1377. [[CrossRef](#)] [[PubMed](#)]
3. Chan, J.; Alegre, T.P.M.; Safavi-Naeini, A.H.; Hill, J.T.; Krause, A.; Gröblacher, S.; Aspelmeyer, M.; Painter, O. Laser cooling of nanomechanical oscillator into its quantum ground state. *Nature* **2011**, *478*, 89–92. [[CrossRef](#)] [[PubMed](#)]
4. Teufel, J.D.; Donner, T.; Li, D.; Harlow, J.W.; Allman, M.S.; Cicak, K.; Sirois, A.J.; Whittaker, J.D.; Lehnert, K.W.; Simmonds, R.W. Sideband cooling of micromechanical motion to the quantum ground state. *Nature* **2011**, *475*, 359–363. [[CrossRef](#)] [[PubMed](#)]
5. Gröblacher, S.; Hammerer, K.; Vanner, M. Observation of strong coupling between a micromechanical resonator and an optical field. *Nature* **2009**, *460*, 724–727. [[CrossRef](#)] [[PubMed](#)]
6. Hao, H.M.; Huang, S.M.; Chen, A.X. Normal mode splitting in a cavity optomechanical system with a cubic anharmonic oscillator. *Int. J. Theor. Phys.* **2021**, *60*, 2766–2777. [[CrossRef](#)]
7. Rabl, P.; Genes, C.; Hammerer, K. Phase-noise induced limitations on cooling and coherent evolution in optomechanical system. *Phys. Rev. A* **2009**, *80*, 063819. [[CrossRef](#)]
8. Gu, W.J.; Li, G.X.; Yang, Y.P. Generation of squeezed states in a movable mirror via dissipative optomechanical coupling. *Phys. Rev. A* **2013**, *88*, 013835. [[CrossRef](#)]
9. Safavi-Naeini, A.; Gröblacher, S.; Hill, J. Squeezed light from a silicon micromechanical resonator. *Nature* **2013**, *500*, 185–189. [[CrossRef](#)]
10. Safavi-Naeini, A.H.; Alegre, T.P.M.; Chan, J.; Eichenfield, M.; Winger, M.; Lin, Q.; Hill, J.T.; Chang, D.E.; Painter, O. Electromagnetically induced transparency and slow light with optomechanics. *Nature* **2011**, *472*, 69–73. [[CrossRef](#)]
11. Field, J.E.; Hahn, K.H.; Harris, S.E. Observation of electromagnetically induced transparency in collisionally broadened lead vapor. *Phys. Rev. Lett.* **1991**, *67*, 3733. [[CrossRef](#)]
12. Harris, S.E.; Field, J.E.; Kasapi, A. Dispersive properties of electromagnetically induced transparency. *Phys. Rev. A* **1992**, *46*, R29. [[CrossRef](#)]

13. Agarwal, G.S.; Huang, S.M. Electromagnetically induced transparency in mechanical effects of light. *Phys. Rev. A* **2010**, *81*, 041803. [[CrossRef](#)]
14. Stephen, E.H. Electromagnetically induced transparency. *Phys. Today* **1997**, *50*, 36. [[CrossRef](#)]
15. Brenda, A.; Alon, B. Double Fano resonance in a plasmonic double grating structure. *Opt. Express* **2016**, *24*, 22334–22344. [[CrossRef](#)]
16. Ferraro, A.; Lio, G.E.; Bruno, M.D.L.; Nocentini, S.; De Santo, M.P.; Wiersma, D.S.; Riboli, F.; Caputo, R.; Barberi, R.C. Hybrid camouflaged anticounterfeiting token in a paper substrate. *Adv. Mater. Technol.* **2023**, *8*, 2201010. [[CrossRef](#)]
17. Nikitas, P.; Nikolay, I.Z. Metamaterial-induced transparency: Sharp Fano resonances and slow light. *Opt. Photonics News* **2009**, *20*, 22–27. [[CrossRef](#)]
18. Weis, S.; Rivière, R.; Deléglise, S.; Gavartin, E.; Arcizet, O.; Schliesser, A.; Kippenberg, T.J. Optomechanically induced transparency. *Science* **2010**, *330*, 1520–1523. [[CrossRef](#)]
19. Teufel, J.D.; Li, D.; Allman, M.S.; Cicak, K.; Sirois, A.J.; Whittaker, J.D.; Simmonds, R.W. Circuit cavity electromechanics in the strong-coupling regime. *Nature* **2011**, *471*, 204–208. [[CrossRef](#)]
20. Karuza, M.; Biancofiore, C.; Bawaj, M.; Molinelli, C.; Galassi, M.; Natali, R.; Tombesi, P.; Di Giuseppe, G.; Vitali, D. Optomechanically induced transparency in a membrane-in-the-middle setup at room temperature. *Phys. Rev. A* **2013**, *88*, 013804. [[CrossRef](#)]
21. Fan, L.R.; Fong, K.Y.; Poot, M.; Tang, H.X. Cascaded optical transparency in multimode-cavity optomechanical systems. *Nat. Commun.* **2015**, *6*, 5850. [[CrossRef](#)] [[PubMed](#)]
22. Dong, C.H.; Zhang, J.T.; Fiore, V.; Wang, H. Optomechanically induced transparency and self-induced oscillations with Bogoliubov mechanical modes. *Optica* **2014**, *1*, 425–428. [[CrossRef](#)]
23. Shen, Z.; Dong, C.H.; Chen, Y.; Xiao, Y.F.; Sun, F.W.; Guo, G.C. Compensation of the kerr effect for transient optomechanically induced transparency in a silica microsphere. *Opt. Lett.* **2016**, *41*, 1249–1252. [[CrossRef](#)] [[PubMed](#)]
24. Burek, M.J.; Cohen, J.D.; Meenehan, S.M.; El-Sawah, N.; Chia, C.; Ruelle, T.; Meesala, S.; Rochman, J.; Atikian, H.A.; Markham, M.; et al. Diamond optomechanical crystals. *Optica* **2016**, *3*, 1404–1411. [[CrossRef](#)]
25. Jing, H.; Özdemir, S.K.; Geng, Z.; Zhang, J.; Lv, X.Y.; Peng, B.; Yang, L.; Nori, F. Optomechanically-induced transparency in parity-time-symmetric microresonators. *Sci. Rep.* **2015**, *5*, 9663. [[CrossRef](#)]
26. Xiong, H.; Si, L.G.; Zheng, A.S.; Yang, X.X.; Wu, Y. Higher-order sidebands in optomechanically induced transparency. *Phys. Rev. A* **2012**, *86*, 013815. [[CrossRef](#)]
27. Kronwald, A.; Marquardt, F. Optomechanically induced transparency in the nonlinear quantum regime. *Phys. Rev. Lett.* **2013**, *111*, 133601. [[CrossRef](#)]
28. Jiao, Y.F.; Lu, T.X.; Jing, H. Optomechanical second-order sidebands and group delays in a kerr resonator. *Phys. Rev. A* **2018**, *97*, 013843. [[CrossRef](#)]
29. Wang, H.; Gu, X.; Liu, Y.X.; Miranowicz, A.; Nori, F. Optomechanical analog of two-color electromagnetically induced transparency: Photon transmission through an optomechanical device with a two-level system. *Phys. Rev. A* **2014**, *90*, 023817. [[CrossRef](#)]
30. Lv, H.; Wang, C.Q.; Yang, L.; Jing, H. Optomechanically induced transparency at exceptional points. *Phys. Rev. Appl.* **2018**, *10*, 014006.
31. Lv, H.; Jiang, Y.J.; Wang, Y.Z.; Jing, H. Optomechanically induced transparency in a spinning resonator. *Photonics Res.* **2017**, *5*, 367–371. [[CrossRef](#)]
32. Zhang, J.Q.; Li, Y.; Feng, M.; Xu, Y. Precision measurement of electrical charge with optomechanically induced transparency. *Phys. Rev. A* **2012**, *86*, 053806. [[CrossRef](#)]
33. Xiong, H.; Si, L.G.; Wu, Y. Precision measurement of electrical charges in an optomechanical system beyond linearized dynamics. *Appl. Phys. Lett.* **2017**, *110*, 171102. [[CrossRef](#)]
34. Lü, X.Y.; Liao, J.Q.; Tian, L.; Nori, F. Steady-state mechanical squeezing in an optomechanical system via Duffing nonlinearity. *Phys. Rev. A* **2015**, *91*, 013834. [[CrossRef](#)]
35. Alvarez, G. Coupling-constant behavior of the resonances of the cubic anharmonic oscillator. *Phys. Rev. A* **1988**, *37*, 4079. [[CrossRef](#)]
36. Jayich, A.M.; Sankey, J.C.; Zwickl, B.M.; Yang, C.; Thompson, J.D.; Girvin, S.M.; Clerk, A.A.; Marquardt, F.; Harris, J.G.E. Dispersive optomechanics: A membrane inside a cavity. *New J. Phys.* **2008**, *10*, 095008. [[CrossRef](#)]
37. Thompson, J.D.; Zwickl, B.M.; Jayich, A.M.; Marquardt, F.; Girvin, S.M.; Harris, J.G.E. Strong dispersive coupling of a high-finesse cavity to a micromechanical membrane. *Nature* **2008**, *452*, 72–75. [[CrossRef](#)]
38. Xia, C.C.; Yan, X.B.; Tian, X.D.; Gao, F. Ideal optical isolator with a two-cavity optomechanical system. *Opt. Commun.* **2019**, *451*, 197–201. [[CrossRef](#)]
39. Huang, S.M.; Hao, H.M.; Chen, A.X. The optomechanical response of a cubic anharmonic oscillator. *Appl. Sci.* **2020**, *10*, 5719. [[CrossRef](#)]
40. DeJesus, E.X.; Kaufman, C. Routh-Hurwitz criterion in the examination of eigenvalues of a system of nonlinear ordinary differential equations. *Phys. Rev. A* **1987**, *35*, 5288. [[CrossRef](#)]
41. Yan, X.B.; Cui, C.L.; Gu, K.H.; Tian, X.D.; Fu, C.B.; Wu, J.H. Coherent perfect absorption, transmission, and synthesis in a double-cavity optomechanical system. *Opt. Express* **2014**, *22*, 4886–4895. [[CrossRef](#)] [[PubMed](#)]

Disclaimer/Publisher's Note: The statements, opinions and data contained in all publications are solely those of the individual author(s) and contributor(s) and not of MDPI and/or the editor(s). MDPI and/or the editor(s) disclaim responsibility for any injury to people or property resulting from any ideas, methods, instructions or products referred to in the content.